

# Design and analysis of a high-accuracy version of the relativity-gyroscope experiment

Benjamin Lange\*

1922 Page Street, San Francisco, California 94117-1804

(Received 18 May 1998; published 23 April 1999)

The detailed design of a high-accuracy orbiting relativity-gyroscope experiment is described, and the performance calculations are given. A pure unsupported gyroscope in a spinning drag-free satellite at ambient temperatures with conventional optical instrumentation can determine the geodetic relativity drift with errors as low as  $0.05 \mu\text{as/yr}$ , an improvement of  $10^3 - 10^4$  over the current GP-B experiment. Recent theoretical work has suggested that under certain assumptions, the deviation of the modified Eddington parameter,  $1 - \gamma \approx 1/\omega_{\text{JBD}}$ , from its value of zero in general relativity should lie in the range  $10^{-4} - 10^{-33}$  with some evidence that the most likely values are between  $10^{-5}$  and  $10^{-9}$ . The experiment described here could measure  $1 - \gamma$  to an accuracy of about  $7 \times 10^{-9}$ , and this would extend the current experimental bound on  $1 - \gamma$  by over five orders of magnitude. In fact, the accuracy may be sufficient to see a massless dilaton as predicted by string theory. In addition if a nearby reference star is chosen, it is sensitive enough to possibly detect Earth-sized planets. The experiment is designed to change altitude and be repeatable, and a series of 1-yr measurements at various altitudes increases confidence in the results, determines the experiment errors, and is necessary for a unique interpretation of the data. [S0556-2821(99)05308-4]

PACS number(s): 04.80.Cc

## I. INTRODUCTION

It is almost certain that general relativity is not the exactly correct theory of gravity because it does not fit into quantum mechanics or any of the force unification schemes and because it predicts space-time singularities. The real question is at what level and in what form will a more exact theory manifest itself, and resolving the mutual incompatibility between general relativity and quantum mechanics would lead to a significant revision of physics. There is no shortage of theoretical attempts to answer this question, some of which are very well motivated. There is, however, a relative dearth of experimental measurements with sufficient accuracy to shed any light on this situation. This paper will describe a highly accurate version of the relativity gyroscope experiment which could help to fill the current gap in experimental results. It would extend the present experimental bound on the deviation from general relativity by over five orders of magnitude, and the accuracy is sufficient to possibly see a massless string dilaton, thus confirming an important prediction of string theory. Until now a description of this version of the experiment known as the autocollimator unsupported gyroscope (AC-USG) has only been available in a very short publication [1] or in a long unpublished analysis [2], and this paper provides a more detailed presentation of the results discussed in [1] and a short summary of [2].

### A. Fourth test

The three classical tests of general relativity proposed by Einstein in 1915–1916 are well known, but it is not generally known that only two years later, in 1918, the Dutch mathematician Schouten proposed a fourth test. Motivated by the realization that the angular momentum vector of a gyroscope free of Newtonian drifts would execute parallel transport as

it moved on a geodesic in curved space, he pointed out that since space was curved by the mass of the Sun, the angular momentum vector of a gyroscope in orbit about the Sun would not point in exactly the same direction after making one complete revolution and that this would manifest itself as a gyroscope drift [3]. He named this the geodetic drift and suggested that the Earth could be regarded as a gyroscope and the drift of its spin axis used to test this effect. Unfortunately, he based his calculation on the curvature of space and not space-time and only got two-thirds of the correct answer. In 1920, Fokker published a paper correcting this error and giving the correct value of 19.2 mas/yr for the geodetic relativity drift due to the Earth's orbital motion [4]. Fokker's expression for the geodetic drift had actually been published in 1916 by de Sitter [5] in connection with the relativistic precession of the Moon's node, but he did not explicitly recognize that this was true for gyroscopes in general or that the phenomenon was based on parallel transport in curved space-time. (See also [6] for an excellent discussion of geodetic drift including the two-thirds error.) Because of the uncertainty in the classical drift of the Earth's spin axis and the inaccuracy of the measurements, it was not possible to perform this test in Schouten's and Fokker's time. In the last 25 years, however, laser reflectors on the Moon's surface and the Viking Mars Lander combined with the highly accurate JPL lunar and planetary ephemerides have made it possible to test both de Sitter's nodal drift and the Schouten-Fokker spin-axis drift to about 0.4 mas/yr, giving a relative accuracy for the geodetic drift of about 2%.

Soon after the launch of the first satellites, it was realized independently and almost simultaneously by two researchers that a precision instrument gyroscope in space could be used to do Schouten's experiment. In an unpublished internal Department of Defense memo in 1959, Pugh suggested using a gyroscope in space to test general relativity [7], and at Stanford University, Schiff (motivated by an advertisement in the December 1959 issue of *Physics Today* for the cryogenic-

\*Email address: blange@sanfrancisco.net

gyroscopic research program at JPL published a similar suggestion in 1960 [8].

### B. Relativity-gyroscope drifts

The relativity drift of a gyroscope consists of two parts: the geodetic drift and the frame-dragging, gravitomagnetic, or Lense-Thirring [9] drift. In order to evaluate the scientific value of an orbital gyroscope experiment, it is useful to write the expression for the gyroscope drift in a form which also includes alternatives to general relativity. If  $\phi_g$  is the geodetic and  $\phi_{fd}$  the frame-dragging drift angle, then in the parametrized post-Newtonian (PPN) formulation of metric theories of gravity the drift of a perfect gyroscope in orbit around a spherical Earth with no other astronomical bodies present is

$$\dot{\phi}_g = \left( \gamma + \frac{1}{2} \right) \frac{\mathbf{v} \times \mathbf{g}}{c^2} = \left( \gamma + \frac{1}{2} \right) \frac{M_\oplus G \mathbf{h}}{c^2 r_s^3} = \left( \gamma + \frac{1}{2} \right) \frac{(M_\oplus G)^{3/2} \hat{\mathbf{h}}}{c^2 r_s^{5/2}} \quad (1)$$

and

$$\dot{\phi}_{fd} = - \left( \frac{\gamma + 1}{2} + \frac{\alpha_1}{8} \right) \frac{[\mathbf{J}_\oplus - 3\hat{\mathbf{r}}_s(\hat{\mathbf{r}}_s \cdot \mathbf{J}_\oplus)]G}{c^2 r_s^3}, \quad (2)$$

where  $\mathbf{v}$  is the instantaneous satellite velocity,  $\mathbf{g}$  is the acceleration of gravity,  $M_\oplus$  is the mass of the Earth,  $\mathbf{J}_\oplus$  is the Earth's angular momentum,  $\mathbf{h}$  is the specific orbit angular momentum,  $\mathbf{r}_s$  is the radius vector of the satellite, and the caret indicates the corresponding unit vector. The first term in Eq. (1) is more general than the last two and is valid for any gravitational field  $\mathbf{g}$ , not just the field from a spherical body.  $\gamma$  is the Eddington parameter, and  $\gamma$  and  $\alpha_1$  together are a subset of the Will-Nordtvedt *parametrized post-Newtonian* parameters [10]. Within the context of PPN theory,  $\gamma$  and  $\alpha_1$  are the quantities which the experiment would measure. In general relativity,  $\gamma=1$  and  $\alpha_1=0$ . In the Jordan-Brans-Dicke (JBD) [11,12,13,10] and other scalar-tensor theories with  $\omega_{\text{JBD}}$  as the coupling parameter,  $\gamma = (\omega_{\text{JBD}} + 1)/(\omega_{\text{JBD}} + 2)$  and  $\alpha_1 = 0$ . Radar time-delay experiments from the Mars Viking Lander [14,10] and the average of a large number of VLBI gravitational-deflection experiments [15,10] give  $|1 - \gamma| < 0.002$ , and solar system measurements [10] have shown  $|\alpha_1| < 4 \times 10^{-4}$ . For large  $\omega_{\text{JBD}}$ ,  $1 - \gamma \approx 1/\omega_{\text{JBD}}$  so that these measurements now put a lower bound on  $\omega_{\text{JBD}}$  of 500.

In a circular orbit,  $\phi_g$  grows at a constant rate, but  $\phi_{fd}$  also contains periodic terms in two times the orbit frequency. As now planned, the experiment would measure the accumulated average<sup>1</sup> growth of  $\phi_{fd}$ . For a spherical Earth and a

<sup>1</sup>The amplitude of the periodic terms at 1500 km is about 1.5  $\mu\text{as}$ , and the experiment is sensitive enough to see them. This would avoid the problem of the proper motion of the star, but as of this time, no study has been made of other twice-orbit error sources. Thus this possibility has not yet been seriously considered. If these errors turn out to be reasonable, this would open the possibility of measuring frame dragging to a few percent without knowing the star's proper motion in right ascension.

TABLE I. Relativity drifts versus orbit altitude.

Orbit altitude (km)	Orbital aberration (mas/yr)	Geodetic drift (mas/yr)	Frame-dragging drift (mas/yr)
0	5444	8444	54.77
650	5186	6623	40.92
750	5149	6393	39.22
1000	5061	5865	35.36
1500	4898	4977	29.04
2000	4749	4267	24.14
2500	4613	3691	20.29
3000	4489	3218	17.21
5000	4075	1984	9.63

circular orbit, the average value of the frame-dragging drift is given by

$$\overline{\phi}_{fd} = \left( \frac{\gamma + 1}{2} + \frac{\alpha_1}{8} \right) \frac{[\mathbf{J}_\oplus - 3\hat{\mathbf{h}}(\hat{\mathbf{h}} \cdot \mathbf{J}_\oplus)]G}{2c^2 r_s^3}. \quad (3)$$

Table I shows some typical values of the geodetic and average frame-dragging drifts for a gyroscope in a circular polar orbit with its spin axis in the plane of the orbit and perpendicular to the Earth's angular velocity. The orbital aberration of starlight is also shown since it will be used to achieve the measurement null.

### C. Significance of the experiment

Although in the final analysis the results of any measurement speak for themselves, it is always good practice to design an experiment in the light of the best theoretical knowledge available. In the case of gravity, almost all modern theories predict the existence of one or more additional scalar sources of the gravitational field. These include generalized Jordan-Brans-Dicke theory, Kaluza-Klein theories, ten-dimensional supergravity (the Chapline-Manton equations [16]), and the low-energy limit of string theory [17]. The problem with the existence of a scalar field has been that its "natural" value would be so large as to be in strong disagreement with experiment. Recently, however, Damour and Nordtvedt published two papers [18,19] which showed that there is a generic mechanism in scalar-tensor theories which, except during radiation dominance, causes them to converge to general relativity as the universe expands; i.e.,  $\omega_{\text{JBD}}$  goes to infinity and  $1 - \gamma$  goes to zero. Later, it was shown by Damour and Polyakov [20] that under the assumption that the various coupling functions all have extrema at a single value of the field, the same result also applies to the string dilaton. Motivated by the fact that extended inflation [21] must terminate with  $1 - \gamma$  of order unity to work at all, they calculated numerical estimates of the present value of  $1 - \gamma$  on the assumption that its value was 1 at the end of inflation and hence also 1 at the end of the radiation era. The Damour-Nordtvedt-Polyakov papers showed that at the present epoch,  $1 - \gamma$  should lie in the range  $10^{-4} > 1 - \gamma > 10^{-8}$  for the JBD scalar field with the most likely values being  $10^{-5} - 10^{-7}$ , and that for a string dilaton, the present value should be

$10^{-6} > 1 - \gamma > 10^{-19}$  with the most likely values<sup>2</sup> being  $10^{-6} - 10^{-9}$ . The important question still remains, however, whether the assumption of  $1 - \gamma$  of order unity at the end of inflation is valid, and recently Damour and Vilenkin published a paper [23] showing that under the assumption that  $1 - \gamma$  was of order unity at the beginning of inflation, the Damour-Nordtvedt mechanism implies a strong dilution of a scalar field during inflation, but that quantum creation of dilatons toward the end or just after inflation would still leave a residual scalar field, which would give a value of  $1 - \gamma$  of the order of  $10^{-21} - 10^{-33}$  at the current epoch.

Thus the theoretical situation concerning what value of  $1 - \gamma$  might be expected at the present time is unclear, but there are still several results which are on reasonably solid ground.

(1) The Damour-Nordtvedt mechanism predicts that, except for the radiation era, the scalar fields will decay as the universe expands. This in turn has two important consequences: first, one can no longer rule out scalar-tensor theories because of solar system measurements which show that<sup>3</sup>  $\omega_{\text{JBD}}$  is greater than 500 or that fundamental constants do not vary with time, etc., and second, the Damour-Nordtvedt mechanism run backwards implies that any scalar field was much larger in the early universe, perhaps leading to pure scalar gravity at some very early epoch. Thus a measurement of  $1 - \gamma$  even at the  $10^{-8}$  level would not merely be a correction to relativity in the eighth decimal place, but would completely alter inflation and preinflation physics.

(2) If  $\Delta a/a$  represents the violation of the equivalence principle, the Damour-Polyakov paper [20] derives a connection between  $1 - \gamma$  and  $\Delta a/a$  which is proportional to the logarithm of the string mass scale. Thus, within the context of the Damour-Polyakov result, a measurement of both  $1 - \gamma$  and  $\Delta a/a$  would measure the string mass scale [24]. If this scale is of the order of  $3 \times 10^{17}$  GeV, the relation between  $1 - \gamma$  and  $\Delta a/a$  is about  $10^{-5}$ , so that, for example, if the equivalence principle has been measured to be smaller than  $10^{-12}$  and if the Damour-Polyakov calculation is correct,  $1 - \gamma$  must be less than  $10^{-7}$ .

(3) The laws of physics during the inflationary era are poorly known with the result that any conclusion based on a calculation during inflation is unreliable. In particular, with varying relative coupling between the scalar and tensor sources of the gravitational field over the history of the uni-

verse, it is not clear at what epoch they should be set equal, i.e., at what epoch  $1 - \gamma$  is of order unity.

(4) If one believes in extended inflation, however, it follows by combining the Damour-Nordtvedt and Darmour-Polyakov calculations that  $10^{-4} > 1 - \gamma > 10^{-19}$ , with  $10^{-5} - 10^{-9}$  being the most likely, and given the correctness of the Damour-Polyakov result, it follows from equivalence-principle measurements that  $1 - \gamma < 10^{-7}$  [26]. Thus any measurement of  $1 - \gamma$  in the range of  $10^{-4} - 10^{-9}$  would have important consequences for string theory and for the mechanism of inflation.

It is possible to draw two general conclusions from the above considerations: (1) In the light of modern theoretical research, the most important emphasis for the relativity-gyroscope experiment is the measurement of  $\gamma$ . (2) High accuracy, at least  $10^{-7}$ , is crucial. Because of these considerations and because an altitude dependence for the geodetic drift of  $r_s^{-5/2}$  is necessary to uniquely identify a scalar field [24], this paper will concentrate almost exclusively on the version of the experiment which consists of a series of high-precision 1-yr measurements of the geodetic drift in altitude increments of 100 km. A method for performing an accurate ( $\sim 10^{-6}$ ) measurement of frame dragging was presented at the Eighth Marcel Grossmann Conference in Jerusalem [27] and will not be discussed here. In addition to the possibility discussed above, that any scalar field was very much larger in the past, finding an additional scalar source of the gravitational field of any size would radically alter the standard model and be of profound importance to fundamental physics.

In addition to the search for a nonzero value of  $1 - \gamma$  represented by the relativity-gyroscope experiments GP-B [28] and the approach described in this paper, there are two designs for satellite-based equivalence-principle experiments, MiniSTEP [29], which promises an accuracy of  $10^{-18}g$  after a run of  $3 \times 10^4$  s, and a new design [30,31] with the potential of  $10^{-22}g$  with the same run time as MiniSTEP or  $10^{-24}g$  with a run time of  $10^8$  s. If the Damour-Polyakov relation  $\Delta a/a \approx 10^{-5}(1 - \gamma)$ , is correct, an equivalence-principle experiment with an accuracy of  $10^{-24}g$  could measure  $1 - \gamma$  to an accuracy of  $10^{-19}$ . It should be emphasized, however, that gyroscope drift and equivalence-principle determinations are independent measurements, and the only way to settle the questions brought out in this section is to actually fly the experiments.

#### D. Description of the relativity-gyroscope experiment

The basic experiment would consist of placing a high-quality gyroscope in orbit about the Earth with its spin axis initially aligned with a distant star and then measuring the angle between the gyroscope and the star versus time. In order to prevent nodal regression from significantly changing the orientation of the plane of the orbit with respect to the gyroscope, the experiment must be done in either an equatorial or a polar orbit. Since both relativity drift vectors are collinear in an equatorial orbit, a polar orbit is generally the better choice. From Eqs. (1) and (3), it can be seen that the geodetic and frame-dragging drift vectors are perpendicular

<sup>2</sup>This follows from applying the Damour-Polyakov result to the moduli fields [22].

<sup>3</sup>Recent papers which have calculated that nucleosynthesis places a constraint on  $\omega_{\text{JBD}}$  which is extremely large are almost certainly wrong [24,25,22]. In fact, it is relatively easy to show [24] that even a constraint  $|\xi| \leq 1.02$  only places a limit on  $1 - \gamma$  at the end of the radiation era of approximately  $0.1\kappa$ , where  $\kappa$  is the Damour-Nordtvedt curvature parameter [18], which is expected to lie between 1 and 10. Although the exact results have yet to be calculated, it is not expected that the recent supernova results measuring the possible existence of a cosmological constant will materially change the estimates of  $1 - \gamma$  given by Damour *et al.* [22].

in a polar orbit so that there are two possible ways to do the experiment: (1) both drifts are measured simultaneously with the gyroscopic spin in the nominal orbit plane, or (2) frame dragging is measured separately with the gyroscope spin perpendicular to the nominal orbit plane. In the first case the measured value of the frame-dragging drift is proportional to the cosine of the reference star's declination and is somewhat masked by the geodetic drift, which is 160 times as large. In the second case setting the gyroscope spin nominally perpendicular to the orbit plane drives the final geodetic drift angle to zero and avoids what is for frame dragging a large error signal. The measurements can either be made with a single gyroscope compared to a star whose proper motion has previously been determined by precision astrometry or two gyroscopes observing the same star can be placed in different orbits so that their relativity drifts are different. The results would then be subtracted to eliminate the uncertainty in the proper motion of the star. The different orbits can either be two counterrotating orbits, two corotating orbits at different altitudes, or a polar orbit and an equatorial orbit.

Barring some unforeseen breakthrough in astrometry, it will be necessary to use two experiments in separate orbits to remove the reference stars proper motion since both current and presently foreseen future astrometric measurements cannot give sufficient accuracy. For a measurement of the geodetic drift, the best choice is two counterrotating orbits with the gyroscope spin axes in the plane of the orbits, and for a frame-dragging experiment, two corotating orbits at different altitudes with the gyroscope spins perpendicular to the nominal orbit planes are best [27]. When differing orbits combined with subtraction are used to eliminate the proper motion of the star, the drift is not measured with respect to the distant stars, but with respect to an inertial reference defined by the initial gyroscope direction. Whether this difference is significant or not is not known at this time.

The experiment analyzed here differs from GP-B in that it operates at ambient temperatures and consists of a single unsupported gyroscope which is maintained in the center of its cavity by small nitrogen-gas jets on the satellite operated by a translation control system; i.e., it is chased by a drag-free satellite [32]. The rotor would be made of single-crystal silicon doped to between 1000 and 100 000 mho/m (0.1–0.001  $\Omega$  cm) so that rotor spin-up and alignment both in inertial and rotor-fixed axes would be accomplished with a three-axis eddy-current induction motor operating between 16 and 160 kHz. The gyroscope spin axis is read out by two redundant two-axis autocollimators looking at small optical flats on the north and south poles of the spherical gyroscope rotor. Zero-point drifts of the instruments are eliminated by rapidly spinning the satellite, and it is this feature which makes low temperatures unnecessary. Using a single unsupported gyroscope instead of four electrically supported gyroscopes has great advantages in terms of drift performance, complexity, reliability, and cost. The question of cross-checking the gyroscope drift will be discussed later (Appendix H 7), and it will be seen that there are a number of better ways to cross-check the drift errors than multiple gyroscopes in one satellite.

Figure 1 shows a schematic view of the 5-cm-diam gyro-

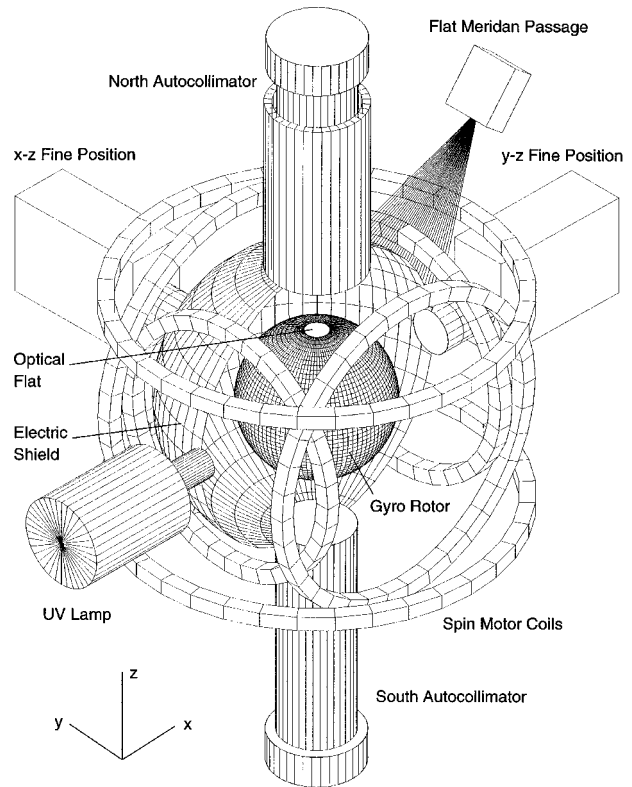


FIG. 1. Gyroscope rotor, autocollimators, spinup coils, cavity wall, etc.

scope rotor, housing, and instruments. The three pairs of coils on orthogonal axes show the three-axis eddy-current induction motor which must perform three functions: spin-up to 924 Hz, active damping (rotation of the spin axis in rotor-fixed coordinates to the normal to the optical flats [33]), and alignment to the star. The two-axis fine-position sensors are autocollimators with the exit beam focused to a point at the center of the rotor, making them sensitive only to translation (transcollimators; cf. Appendix C 4). The UV light would discharge the rotor if needed. The hemisphere behind the rotor is a cutaway of the electric shield and vacuum can, and the array of lines in the far background is an optional fiber-optic bundle to detect the meridian passage of the flats for coarse active damping. The electric shield is divided into three pairs of orthogonal electrodes for coarse position sensing and charge measurement. The gyroscope and instruments are enclosed in a multilayer Mumetal magnetic shield, and this assembly is enclosed together with the two telescopes in a thermally insulating chamber. The satellite would carry sufficient nitrogen control gas for drag-free lifetimes of 10–25 yr and sufficient monopropellant hydrazine for an inclination change of 6° and an altitude change of 1000 km.

Before beginning a detailed analysis of the experiment performance, it is useful to make a few remarks about microarcsecond measurements in general. A microarcsecond ( $\mu$ as) is very small,  $5 \times 10^{-12}$  rad, and the question naturally arises as to whether or not measurements at this level are possible at all. In this connection it should be pointed out that a number of groups have looked at microarcsecond measurements in space with optical instruments and have con-

cluded that they are possible. Reasenberg and a very large number of coauthors [34] have published a study on the POINTS project, which concludes that it can measure position and parallax to  $0.6 \mu\text{as}$  and proper motion to  $0.4 \mu\text{as}/\text{yr}$ , and Shao at JPL is planning similar accuracies with OSI [35]. As early as 1959, Jones and Richards [36] reported an optical lever with a noise-equivalent angle of about  $14 \mu\text{as}/\text{Hz}^{1/2}$ , which with  $10^4$  sec of averaging gives a measurement noise error of about  $0.1 \mu\text{as}$ . Furthermore, the VLBI group responsible for joining the radio and Hipparcos references is now measuring some radio stars with a precision of tens of microarcseconds [37]. For the gyroscope experiment it can be shown that instrument noise levels of a few  $\mu\text{as}/\text{Hz}^{1/2}$  are possible, so that the principal problem is to design an experiment whose accuracy is limited only by the noise. This is done primarily by doing all measurements in null to the maximum extent possible, using satellite spin to greatly reduce any instrument zero-point drifts, subtracting the gyroscope readout from the telescope readout to eliminate satellite attitude errors, and by having a method of accurately calibrating the region smaller than the size of the null. The aberration of starlight will be used both to cancel the relativity drift to achieve measurement in null and to calibrate the autocollimator and telescope scale factors. Reduced to its simplest terms, the problem boils down to measuring up to  $\pm 0.2$  arcsec (the null size) with an accuracy of about  $0.2 \mu\text{as}$ . Because of the amplification of a thin tipping plate, this becomes a problem of measuring  $\pm 10^\circ$  with an accuracy of  $0.04$  arcsec.

To determine the system performance and hence the experiment accuracy, there are basically four items to check: (1) the classical gyroscope drift errors, (2) the autocollimator noise equivalent angle and scale-factor errors, (3) the telescope performance including the noise equivalent angle and scale-factor calibration, and (4) the roll-coupled errors which show up as zero-point errors or drifts. In addition, there are many ancillary issues which must be looked at. These include active damping during rotor spinup, the fabrication and measurement of the rotor, details of the orbits which cancel the gravity-gradient drift, the use of aberration of starlight to cancel the relativity drift angles, operational considerations, etc.

In this paper all noise spectral densities and power spectral densities are one sided, and if the densities are assumed to be white over the range of interest, the error angle is given by the power spectral density divided by the square root of the averaging time times 2. The use of very long averaging times to achieve high accuracy is acceptable provided that the noise is truly white and that the quantity to be extracted from the noise is either constant or has a known or determinable variation with time.

The reference frames used to describe the experiment have their  $z$  axes nominally in the direction of the star ( $S$  frame) or the gyroscope ( $G$  frame), and their  $x$  axes defined so as to form the smallest possible angle with respect to the Earth's north pole. For most discussions there is no distinction between these two frames, and with these definitions, the experiment measures the  $y$ -geodetic drift so that the  $y$  axis is the experiment axis and the  $x$  axis is the cross axis.

## II. GYROSCOPE DRIFT ERRORS

The drift rate of the AC-USG gyroscope will be shown in this section to be about  $0.04 \mu\text{as}/\text{yr}$ . This extraordinarily low drift corresponds to  $10^{-15}$  deg/h which is ten orders of magnitude better than the best inertial quality gyroscopes that have ever been built on the Earth. How is it possible to get this kind of performance? The most important step is to do the experiment in space where the disturbing torques from the rotor support forces are either very small or nonexistent, but in addition, the satellite spin axis must be controlled to be accurately parallel to the gyroscope spin axis, the rotor should be unsupported (no electric support fields in the cavity), a wide rotor-cavity gap (one cm) should be used, and the orbit should be fine tuned to eliminate gravity-gradient drifts. (See [1] for more details and Appendix B for the orbits.) As a result of the absence of electric support torques, there are only about 24 drift sources. This increases the probability that no important drift source has been forgotten and that the list is exhaustive. Table II summarizes the sources of Newtonian drift,  $\phi$ , of the AC-USG and is an extension of a similar table in Ref. [32].  $a$  is the rotor radius,  $d$  the cavity gap,  $\omega_G$  the gyroscope spin rate,  $n$  the mean orbit rate,  $\rho$  the density of the rotor,  $\sigma$  the rotor conductivity,  $A$  the accuracy of roll averaging,  $V$  the rotor charge potential,  $B$  the magnetic field,  $S_{AC}$  the AC magnetic shielding factor, and  $p$  the cavity pressure,  $\varepsilon_p$  is the permanent rotor moment of inertia difference ratio  $\Delta I_p/I$ , and in general  $\varepsilon$  with the appropriate subscript is any roundness, miscentering, or misalignment factor. The definitions of the rest of the symbols in Table II are given in Appendix A for the important drifts and in [2] and [32] for the minor ones.

For the magnetic drifts, the magnitudes of the drifts in Table II are not given by simply substituting in the corresponding formula, but they must be determined by simulation since they depend on the details of the orbit. The geodetic-relativity, gravity-gradient, eddy-current, and Barnett drifts can be very accurately calculated, and for this reason only the drifts in the experiment axis (the  $y$  axis in the star reference frame) are shown in Table II. This is discussed in more detail in the appendixes. The physical basis for the important drifts and their calculation is explained in Appendix A, and the orbital simulations are presented in Appendix B.

Figure 2 shows the gyroscope drifts as a bar chart. It can be seen that the largest drifts come from gravity gradient, eddy currents, electric fields, gas Brownian motion, flat differential pressure, and large particles. There is no Barnett or spinning-charge drift in the experiment axis ( $y$  axis), but rather a steady oscillation throughout the year at diurnal period with an amplitude of about  $1.3 \times 10^{-6} \mu\text{as}$  superposed on a constant term of the same amplitude. In the cross axis ( $x$  axis), however, there is a steady  $x$ -Barnett drift of about  $-2.9 \times 10^{-2} \mu\text{as}/\text{yr}$ , and for this reason, the Barnett and spinning-charge drifts will be considered among the important drift sources.

In addition to the calculations which support the very low drift of the AC-USG, there is experimental evidence that the gyroscope drifts are really as small as claimed here. In 1972

TABLE II. Summary of drift torque sources and drifts.

Source of torque	Formula for $\dot{\phi}$	Auxiliary formula, critical values, comments, etc.	Drift ( $\mu\text{s/yr}$ )
Gravity gradient	$\dot{\phi}_{\text{av}} = \frac{3}{2} n^2 \left( \frac{\varepsilon_p}{\omega_G} + \frac{k_v \rho a^2}{E} \omega_G \right) \theta_{ml}$	$\varepsilon_p = 10^{-4}$ , compensation = $10^{-3}$ orbits from Appendix B	$3.04 \times 10^{-2}$
S/C gravity gradient	$\dot{\phi}_{\text{av}} = \frac{3}{2} \frac{m_S}{r_S^3} \left( \frac{\varepsilon_p}{\omega_G} + \frac{k_v \rho a^2}{E} \omega_G \right) A$	$A = \text{roll average} = 10^{-7}$ $m_S = 1000 \text{ kg}$ , $r_S = 1 \text{ m}$	$2.24 \times 10^{-3}$
Magnetic eddy currents	$\dot{\phi}_{\text{av}} = \frac{\sigma B_{e\perp} B_{e\parallel} S_{\text{AC}}^2 C_m A_{\text{orbit}}}{4\rho}$	$\sigma S_{\text{AC}}^2 C_m = 10^{-5} \text{ mhos/m}$ , $A_{\text{orbit}}$ from Appendix B	$7.00 \times 10^{-3}$
Barnett effect	$\dot{\phi}_{\text{peak}} = \frac{5 \chi_m H_e S_{\text{AC}} C_{Bn}}{\rho a^2 g_m e / m_e}$	Magnetic susceptibility $\chi_m = -3.7 \times 10^{-6}$ , $S_{\text{AC}} C_{Bn} = 3 \times 10^{-5}$	$1.20 \times 10^{-5}$
Spinning charge	$\dot{\phi}_{\text{peak}} = \frac{5 \varepsilon_0 V (1 + a/d) B_e S_{\text{AC}} C_{Bn}}{2 \rho a^2}$	$\dot{\phi}_{s, \text{chg}} = -0.920 \left( \frac{V}{1 \text{ V}} \right) \dot{\phi}_{\text{Barnett}}$	$1.10 \times 10^{-4}$
Residual $B_i$ field in shield	$\dot{\phi}_{\text{av}} = \frac{B_{i\perp}^2 \sigma \varepsilon_{\text{att}}}{4\rho}$	$B_{i\perp} = 0.3 \times 10^{-3} \text{ G}$ $= 3 \times 10^{-8} \text{ T} \approx 10^{-3} B_e$ , $\varepsilon_{\text{att}} = 10^{-8}$	$6.26 \times 10^{-3}$
Electric fields in the cavity	$\dot{\phi} = \frac{15 \varepsilon_0 \varepsilon_{\text{sph}} A}{16 \rho a^2 \omega_G} \left[ \frac{V}{d} \left( 1 + \frac{d}{a} \right) \right]^2$	$V_R$ due to charge = $10 \text{ V}$ max, $\varepsilon_{\text{sph}} = 10^{-6}$	$1.25 \times 10^{-3}$
Electric fields with the flats	$\dot{\phi} = \frac{15 \varepsilon_0 \varepsilon_{mc} A}{16 \rho a^2 \omega_G} \left[ \frac{V}{g_{ac}} \left( 1 + \frac{d}{a} \right) \right]^2 \left( \frac{r_f}{a} \right)^3$	$\varepsilon_{mc} = 0.01$ , flat to rotor radius, $r_f/a = 0.1$	$3.11 \times 10^{-3}$
Misaligned gas spin-down torque	$\dot{\phi} = \frac{15 b_{\text{gas}} A \varepsilon_{ml}}{8 \pi \rho a^5}$ $= \frac{5 A \varepsilon_{ml}}{\rho a} p \sqrt{\frac{m_a}{2 \pi k T}}$	$\varepsilon_{ml} = 10^{-4}$ , $p = 10^{-9} \text{ Torr}$	$6.5 \times 10^{-4}$
Gas Brownian drift	$\langle \phi^2 \rangle = \frac{4 b_{\text{gas}} k T t}{h_G^2}$	$b_{\text{gas}} = \frac{8 \pi}{3} a^4 p \sqrt{\frac{m_a}{2 \pi k T}}$	$1.31 \times 10^{-2}$
Differential pressure	$\dot{\phi} = \frac{15 \varepsilon_{\text{sph}} A p}{8 \rho a^2 \omega_G}$	Assume full cavity pressure acts on only one side	$1.92 \times 10^{-5}$
Differential pressure on flats	$\dot{\phi} = \frac{15 \varepsilon_{mc} A p}{8 \rho a^2 \omega_G} \left( \frac{r_f}{a} \right)^3$	Assume full cavity pressure acts on only one flat	$1.92 \times 10^{-3}$
Autocollimator light beam power	$\dot{\phi} = \frac{2 P_{\text{AC}}}{c} \frac{\varepsilon_{\text{mac}} r_f A}{h_G}$	$P_{\text{AC}} = 4 \mu\text{W}$ , Appendix C 1	$1.95 \times 10^{-5}$
Position light beams and UV	$\dot{\phi} = \frac{2(P_{\text{pos}} + P_{\text{UV}})}{c} \frac{\varepsilon_{\text{sph}} a A}{h_G}$	$P_{\text{pos}} = 4 \mu\text{W}$ $P_{\text{UV}} = 6.2 \times 10^{-11} \text{ W}$	$1.95 \times 10^{-9}$
Iron cosmic rays	$\sqrt{\langle \phi^2 \rangle} = \frac{15 \sqrt{\pi}}{32} \frac{F_{e\nu} I_{\text{Fe}}}{c a^2 \omega_G} \sqrt{n_{\text{Fe}} t}$	Ref. [38], p. 575	$1.35 \times 10^{-4}$
South Atlantic Anomaly	20 times the drift from proton cosmic rays [[38], p. 575]		$8.01 \times 10^{-5}$
Solar flares	$\sqrt{\langle \phi^2 \rangle} = \frac{15 \sqrt{\pi}}{32} \frac{F_{e\nu} I_{\text{SF}}}{c a^2 \omega_G} \sqrt{n_{\text{SF}} t}$		$4.51 \times 10^{-5}$
Proton cosmic rays	$\sqrt{\langle \phi^2 \rangle} = \frac{15 \sqrt{\pi}}{32} \frac{F_{e\nu} I_{\text{H}}}{c a^2 \omega_G} \sqrt{n_{\text{H}} t}$		$4.00 \times 10^{-6}$

TABLE II. *Continued.*

Source of torque	Formula for $\dot{\phi}$	Auxiliary formula, critical values, comments, etc.	Drift ( $\mu\text{s/yr}$ )
Photon Brownian drift	$\langle \phi^2 \rangle = \frac{4b_{ph}kTt}{h_G^2}$	$b_{ph} = \frac{32}{5} \left(\frac{\pi}{3}\right)^2 \left(\frac{\pi}{K}\right)^4 \left(\frac{a}{\lambda_m}\right)^4 h$	$8.65 \times 10^{-5}$
Misaligned photon spin-down torque	$\dot{\phi} = \frac{15b_{ph}\epsilon_{ml}A}{8\pi\rho a^5}$		$5.66 \times 10^{-8}$
Large particles	See Appendix A 6	100 collisions per year of 0.5 micron-size particles	$1.65 \times 10^{-2}$
Anisotropic $\chi_m$	$\phi_{\text{peak}} = \frac{5\Delta\chi_m B_s^2}{2\mu_0\rho a^2\omega_G}$	$\Delta\chi_m = 0.1\chi_m$	$5.10 \times 10^{-5}$
Induced magnetic moment in a nonspherical rotor	$\phi_{\text{miscal}} = \frac{5\chi_m B_s^2 \epsilon_{\text{geom}}}{2\mu_0\epsilon_p\rho a^2\omega_G^2}$	$\epsilon_{\text{geom}} = 10^{-5}$	$5.10 \times 10^{-9}$
Einstein-de Haas	$\phi = \frac{5\chi_m H_s}{\rho a^2 (e/m_e) g_m \omega_G}$	An angle, not a drift rate, units are $\mu\text{as}$	$3.06 \times 10^{-13}$
		RSS of all drift sources ( $\mu\text{s/yr}$ )	$3.84 \times 10^{-2}$

the Department of Aeronautics and Astronautics at Stanford University in conjunction with the Applied Physics Laboratory at Johns Hopkins University flew a full three-axis drag-free satellite as part of the Navy's Transit navigation satellite series known as TRIAD I [39]. The design goal for this effort was to achieve a level of drag-free performance such that the specific forces at the proof mass were less than about  $10^{-11}g$ . When the satellite was flown, actual flight test data showed that the specific forces were no larger than  $0.5 \times 10^{-11}g$ . This accomplished two important things: it

showed that the methodology used to calculate the disturbing forces [32] was correct, and it provided an upper bound on the drift that a gyroscope in a very similar cavity to the one proposed here would have had.

The crucial point is that the calculations of the disturbing forces on the proof mass were done from the same list as in this section and were done in the same way. Except for gravity-gradient and magnetic torques, all torques on the gyroscope act through forces applied to the rotor; i.e., the only pure couples arise from gravity gradient and magnetic

**Gyro Drifts**

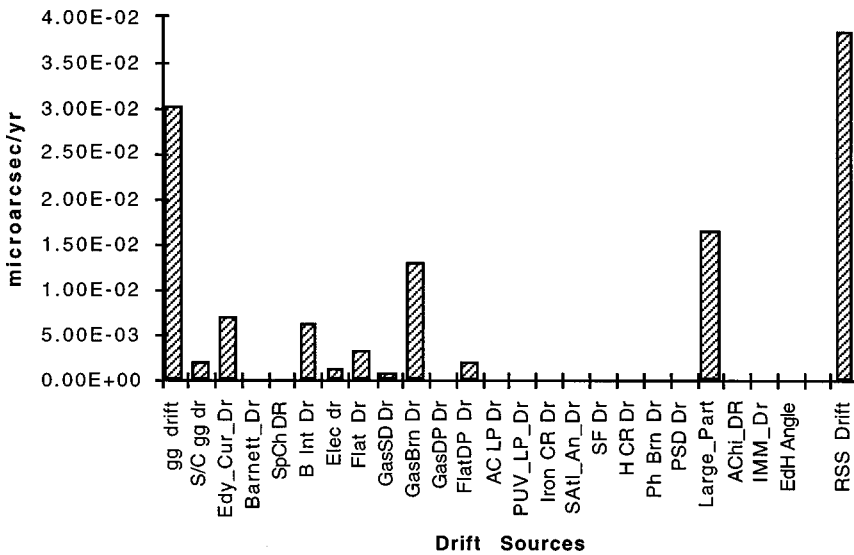


FIG. 2. Gyroscope drifts from the various sources.

effects.<sup>4</sup> The drift caused by a deterministic specific force  $f_{xyz} = 0.5 \times 10^{-11} g$ , acting on a gyroscope of roundness,  $\epsilon_{\text{round}} = 10^{-6}$ , with roll averaging  $A = 10^{-7}$ , is bounded by

$$\dot{\phi} < \frac{5f_{xyz}\epsilon_{\text{round}}A}{2a\omega_G} = 5.5 \times 10^{-7} \text{ } \mu\text{as/yr.} \quad (4)$$

This bound shows that with one exception<sup>5</sup> the 1972 flight puts an experimental limit on all forces which could torque the gyroscope. The AC-USG design uses a 10-mm gap with an optical pickoff, whereas the 1972 design used a capacitive pickoff with a 9-mm gap. The only drift sources which were not tested by the 1972 flight were the gravity-gradient, magnetic, and random-walk torques. These torques, however, are the easiest to analyze because they have the simplest and most accurate mathematical descriptions, and this paper will pay special attention to them in Appendixes A and B.

Thus the 1972 flight results give strong support to the claim that the list of drift sources discussed in this section is exhaustive and that the methodology of calculation is correct. In the case of rotor charge, energetic radiation is believed to charge the rotor at a constant rate [40] and a large charge could eventually build up on the rotor and cause excessive drifts. Although no precautions were taken to avoid proof-mass charge, no evidence for this was seen in the TRIAD I flight. The mechanism by which the proof mass was discharged is unknown, but presumably the same mechanism which charged the proof mass provided an ionizing medium for discharging. In spite of these results, it is still planned to actively discharge the rotor with UV light since the discharge mechanism was unknown and the higher vacuum planned for this flight may not provide a sufficiently discharging ionized medium.

### III. AUTOCOLLIMATOR

The use of an autocollimator reflecting from a rotor flat for the spin-axis readout has a number of advantages over other conceivable competing readout schemes: (1) an autocollimator is existing mature technology and is the scientific and industrywide standard of precision small-angle measurement, (2) it is an ultralow-noise device, (3) it is insensitive to translational motion of the rotor, (4) it can be accurately calibrated on the ground in a laboratory environment, (5) unlike a liquid helium Dewar, it is very small and light weight, and (6) it functions at room temperature and both at atmospheric pressure and in vacuum, making it easy to work

<sup>4</sup>A significant electric dipole moment accompanied by a zero monopole moment is not possible in a conducting spherical rotor.

<sup>5</sup>The exception is random-walk-type drifts caused by molecular, photon, or large particle collisions. In principle, it would have been possible to bound this drift source since it can be shown that random walk in angle and position are connected by  $\sqrt{\langle \phi^2 \rangle} = 4\sqrt{\langle x^2 \rangle}/a\omega_G t$ . No measurement of the random-walk component of the position errors was possible, however, so that the experiment gives no information on this drift source.

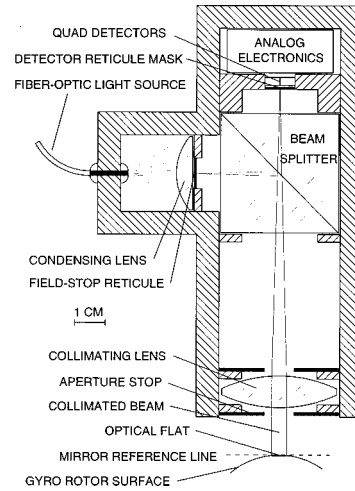


FIG. 3. Gyroscope readout autocollimator.

with in the laboratory and fully functional in space. The details of the autocollimator design and performance are given in Appendix C.

In order to use an autocollimator as the readout, the rotor must be fabricated with two optical flats at each end of the 0-g maximum axis of inertia<sup>6</sup> with the flat normals aligned to this axis. The alignment error of the flats must be less than the linear range of the autocollimator and must not generate an AC signal at spin frequency so large that it swamps the measurement. Thus an important problem for the autocollimator readout is the fabrication of the rotor. This problem was solved in the late 1960s, and this solution is summarized in Appendix D.

Figure 3 shows a drawing of the autocollimator which would be used for the gyroscope readout and illustrates its principle of operation. As can be seen from the figure, when the mirror in the collimated output beam rotates about an axis perpendicular to the beam, the light in the return beam is displaced along the surface of the group of four photodiodes. When the signals of two opposite pairs of photodiodes are subtracted, this produces an output signal proportional to the rotation angle of the mirror. The light source is a fiber-optic bundle which allows chopped high intensity light with very little heating and simplifies the problem of providing a redundant light source. With a 10-cm focal length and a 5-mm optical flat, the focal ratio of the resulting optical system is 20.

For small angles and a constant satellite rotation rate, the  $x$ - and  $y$ -axis angles  $a_x$  and  $a_y$  read out by an autocollimator with unity scale factor looking at a gyroscope rotor spinning at rate  $\omega_G$  in a satellite rolling at rate  $\omega_S$  are

<sup>6</sup>The maximum axis of inertia does not significantly depend on  $g$ , but its measurement in an Earth-bound laboratory does. A body-fixed moment caused, for example, by an offset of the center of mass with respect to the center of support perpendicular to the spin axis gives an apparent rotation of the maximum axis of inertia in a 1-g field.

TABLE III. Autocollimator signals.

Error term	Symbol	Size ( $\mu\text{as}$ )	Frequency (Hz)	Output signal level
Flat misalignment errors	$n_x, n_y$	$10^5$	924	Suppressed by filtering
Satellite attitude errors	$\gamma_x, \gamma_y$	$10^3$	0.16	Angles to be measured
Rotor polhode amplitude	$\alpha_p$	$10^3 - 10^5$	924	Suppressed by filtering
Zero-point errors	$b_x, b_y$	Set < 100	dc	Suppressed by filtering

$$a_x = n_x \sin \omega_{G-S} t + n_y \cos \omega_{G-S} t - \alpha_p \\ \times \sin[(\Omega + \omega_{G-S})t + \phi] + \gamma_x + b_x$$

and

$$a_y = -n_x \cos \omega_{G-S} t + n_y \sin \omega_{G-S} t + \alpha_p \\ \times \cos[(\Omega + \omega_{G-S})t + \phi] + \gamma_y + b_y,$$

where  $n_x$  and  $n_y$  are the flat misalignment errors (the  $x$  and  $y$  components of the flat unit normal in rotor coordinates),  $\alpha_p$  is the instantaneous polhode angle,  $\omega_{G-S}$  is the difference angular velocity between the gyroscope rotor and the satellite,  $\Omega$  is the polhode angular velocity,  $\phi$  is the initial phase of the rotor  $x$  and  $y$  angular velocities,  $\gamma_x$  and  $\gamma_y$  are the satellite  $z$ -axis angles in satellite-fixed coordinates relative to an inertial reference frame whose  $z$  axis is defined by the gyroscope angular momentum vector, and  $b_x$  and  $b_y$  are the autocollimator bias or zero-point errors.  $\gamma_x$  and  $\gamma_y$  give the satellite attitude relative to the gyroscope and are the quantities which are to be measured by the autocollimator. The satellite attitude control system attempts to drive  $\gamma_x$  and  $\gamma_y$  to zero. If  $\alpha_x$  and  $\alpha_y$  are the inertial satellite attitude errors, i.e., the angles which rotate the gyroscope angular momentum vector (inertial reference  $z$  axis) into the satellite  $z$  axis, then  $\gamma_x = \alpha_x \cos \omega_s t + \alpha_y \sin \omega_s t$  and  $\gamma_y = -\alpha_x \sin \omega_s t + \alpha_y \cos \omega_s t$  so that  $\gamma_x$  and  $\gamma_y$  oscillate at the satellite roll frequency of  $\omega_s/2\pi = 0.16$  Hz. The gyroscope-minus-satellite frequency  $\omega_{G-S}/2\pi$  is almost exactly equal to the rotor spin rate of 924 Hz, and the polhode radian frequency  $\Omega$  equals  $\varepsilon_p \omega_G$ , which gives a polhode period of about 10 sec. Thus the flat misalignment errors  $n_x$  and  $n_y$  and the polhode motion are well separated in frequency from the satellite attitude angles  $\gamma_x$  and  $\gamma_y$ . The approximate amplitudes of the terms are given in Table III. The zero-point errors are set below 100  $\mu\text{as}$  by the automatic mass-trim system and by the electronic bias signal shown in Fig. C2 in Appendix C.

For the autocollimator shown in Fig. 3, the noise equivalent angle is  $8.2 \mu\text{as}/\text{Hz}^{1/2}$ , which, for example, gives a measurement error of 0.06  $\mu\text{as}$  with  $10^4$  sec of averaging. This very low noise is achieved by basing the design on the Jones-Pfund reticule concept. In 1959, Jones and Richards [36] published a description of an optical lever (essentially a single-axis autocollimator) based on his reticule with an experimental noise equivalent angle of  $14 \mu\text{as}/\text{Hz}^{1/2}$  [36]. The principle of the Jones design and the performance of the gyroscope readout autocollimator is discussed in detail in Appendix C. Although the noise angle derived in Appendix

C is only a calculated value, it should be emphasized that the performance reported by Jones was an experimental result obtained in air at room temperature. Appendix C also gives more detail on the separation of  $\gamma_x$  and  $\gamma_y$  from the other signals.

#### IV. TELESCOPE

At this time for the purpose of this article, the telescope is assumed to be a 40-cm Schmidt-Cassegrain with a focal length of 10 m read out by one or two thin servo-controlled tipping plates rigidly attached to angle encoders. Rotation of the fine tipping plates translates the focused image of the star on a pyramid prism. The image is centered on the tip by a servo controller which rotates the plate, and this rotation is read out by the angle encoder. Because a large rotation of the fine tipping plate results in only a very small translation of the image, very small angle changes can be read out with a standard angle encoder modified to include analog division of the least significant bit. The coarse tipping plates<sup>7</sup> are able to make coarse alignment adjustments of approximately  $\pm 2$  minutes of arc. This would be used to align the telescope zero point with the autocollimators just before the precision measurements, and the coarse tipping plates would then be locked. Besides setting the zero point, they also make it possible to take low-precision data during the entire year when the annual aberration angles are out of null. The focal ratio of the optics is 25, and the field of view is 10 arcsec. Since the diameter of the diffraction circle is about 0.3 arcsec, the total field of view is about 30 times as large as the diffraction circle.

A low-noise equivalent angle in the telescope is achieved by using as large a telescope as practical and by looking at a bright star. The use of the bright stars whose proper motion uncertainty is typically of the order of 1 mas/yr is made possible by the elimination of proper motion through the subtraction of separate experiments in two orbits. Solving the problem of proper motion was especially difficult. This can be illustrated by an imaginary relatively-gyroscope experiment performed by someone living 30 parsecs from our Sun

<sup>7</sup>Tipping plates are used instead of mirrors or a two-axis adjustable secondary because they give a much smaller change in angle adjustment for a given rotation. Multiple reflections are an added complication, but they can be removed by biasing the coarse tipping plates at an offset angle. In the case of the fine tipping plates, multiple reflections may require the use of a single two-axis plate instead of two single-axis plates.

who decided to use it as his reference star. The linear proper motion could be backed out of the data with a series of measurements in 100-km-altitude increments, but just Jupiter would cause the Sun to move in a circle with an apparent diameter of  $140 \mu\text{as}$  and an unknown period of 11.9 yr. Thus without counterrotating orbits, it is impossible to do a gyroscope experiment at the  $1\text{-}\mu\text{as}$ -accuracy level without knowing the planetary structure of the reference star, a clearly impossible requirement at this time.

The telescope performance is calculated in detail in Appendix E, which lists the results for several stars and two different photomultipliers using a 40-cm telescope. The noise angle varies between about 6 and  $20 \mu\text{as}/\text{Hz}^{1/2}$ , depending on the star, and  $10 \mu\text{as}/\text{Hz}^{1/2}$  is chosen as a typical value for the calculation of the overall experiment accuracy. In order to achieve an absolute angle accuracy comparable with the noise, the scale-factor errors must be calibrated to the same accuracy. During the time that the counterrotating orbits are being established, there is about a year available to do a preliminary scale-factor calibration (cf. Sec. VI). In addition, in order not to require an unreasonable scale-factor accuracy, it is necessary that the linear range over which the measurements are made be less than about 0.2 arcsec. This is accomplished by using the orbital aberration of starlight also to cancel the relativity drift. For orbits higher than 1560 km, the geodetic relativity drift is less than the orbital aberration, and exact cancellation is possible. Because the annual aberration of starlight is also present and can be as large as 40 arcsec, precision data can only be taken at the beginning and the end of the year when the annual aberration returns to its starting value. The details of how this is done are also explained in Appendix E. The important question arises as to how long the annual aberration allows the cancellation within 0.2 arcsec to hold since this determines the amount of averaging time available to reduce the noise. It is shown in Appendix E that the apparent angle between the reference star and gyroscope can be made to remain within 0.2 arcsec for about 23 days at the beginning and the end of the experiment giving an effective noise averaging time of about 43 000 sec. The full 23 days is not available for averaging since the orbital aberration only allows data to be taken during a relatively short part of the orbit. The results of the calculations in Appendix E are summarized in Sec. VII on the experiment accuracy.

## V. ROLL-FREQUENCY ERRORS

In a nonspinning satellite, if the point at which either the autocollimator or the telescope reads zero were to shift over the course of a year, this would be interpreted as a gyroscope drift and would contribute directly to an error in the experiment. Spinning the satellite shifts all inertially fixed signals such as the difference between the direction to the reference star and the direction of the gyroscope angular momentum vector to the satellite spin frequency, leaving all satellite-fixed errors such as electronic and mechanical zero shifts, partial darkening of the optics, detector degradation, thermal bending, etc., at zero frequency. It is this property which eliminates the need for very low temperatures to “freeze” the instrument zero points for the 1-yr duration of the experi-

ment. Instead, the instrument zero points must only be stable for about one spin period of 6 sec.

Any zero-point error, however, which had a component at satellite spin frequency and which changed over the course of a year would cause an experiment error. Because of the very high accuracy requirements of the experiment, these errors must be carefully investigated. In Appendix F it is shown that the errors at satellite spin frequency from all sources are less than about  $0.01 \mu\text{as}$ .

## VI. INSTRUMENT CALIBRATION

The discussion of the scale-factor errors in Appendixes C3 and E3 concentrates on techniques for reducing the scale-factor errors by making the linear range over which data are taken as small as possible so that the experiment can operate as close to null as possible. In the case of the autocollimator, this is done by separating the disturbing signals in frequency and by designing the satellite attitude control to track the gyroscope with a very small error. For the telescope, the linear range is reduced by using the orbital aberration of starlight to cancel the relativity drift and by only taking data at the beginning and end of the year when the annual aberration has returned to its starting value. In this case the key trade-off is between the amount of time available for averaging and the size of the linear range. A larger linear range gives more averaging time, but it increases the scale-factor errors. A compromise value of 0.2 arcsec has been chosen as a balance between these two factors. While 0.2 arcsec may seem small, it is  $200\,000 \mu\text{as}$ , and for an experiment with submicroarcsecond accuracy, the same calibration problem as with any non-null experiment is present. In spite of averaged instrument noise levels well below  $1 \mu\text{as}$ , an overall accuracy this low would be a hopeless problem were it not for the fact that a precision calibration signal with an accuracy of  $0.014 \mu\text{as}$  is available in the orbital aberration of starlight.<sup>8</sup> This is possible because modern Earth satellite tracking systems achieve extremely high accu-

<sup>8</sup>All aberration errors other than the satellite’s orbital velocity relative to the Earth become common-mode errors and are eliminated when the results of two experiments in two orbits are subtracted. In an experiment which does not do this, but rather uses precision astrometry to find the proper motion of the star, the additional aberration errors come from three sources: the motion of the Earth relative to the Sun, the orbital motion of the Sun with neighboring stars, and the change in the direction of the velocity caused by galactic rotation. The velocity changes of the reference star are not important since only light that departs at an angle which exactly cancels the star’s aberration can arrive at the telescope. Finally, only changes in the above velocities cause errors. The velocity error in the Earth’s orbit is approximately  $5 \times 10^{-5}$  m/sec, corresponding to an aberration error of  $0.035 \mu\text{as}$  [41]. The error from the Sun’s orbital motion with respect to its neighbors can be calculated to be roughly  $0.002 \mu\text{as}$ . The velocity direction change due to galactic rotation is surprisingly large, about  $4 \mu\text{as}/\text{yr}$ , which can be compensated to about  $0.8 \mu\text{as}/\text{yr}$ . Errors caused by other masses in the local group of galaxies are completely negligible, being of the order of  $10^{-14} \mu\text{as}$ .

TABLE IV. Experiment errors.

Source	Error	Units	Comments
Gyroscope drift	0.040	$\mu\text{as/yr}$	Table II
Proper motion	0	$\mu\text{as/yr}$	Counter rotating orbits
Geodetic-drift-calculation error	0.079	$\mu\text{as/yr}$	Table A2
Autocollimator (AC) noise density	8	$\mu\text{as/Hz}^{1/2}$	Appendix C 1
Effective AC noise averaging time	21500	sec	Telescope time/2 (chopping)
Autocollimator noise error	0.039	$\mu\text{as}$	Noise/ $(2T_{\text{av}})^{1/2}$
Weighted AC scale factor	0.03	$\mu\text{as}$	Appendix C 3
One-half the AC unmodeled errors	0.025	$\mu\text{as}$	
Telescope noise density	10	$\mu\text{as/Hz}^{1/2}$	Table E1
Effective telescope noise averaging time	43000	sec	Effective null time
Telescope noise error	0.034	$\mu\text{as}$	Noise/ $(2T_{\text{av}})^{1/2}$
Weighted telescope scale factor error	0.03	$\mu\text{as}$	Appendix G
One-half the telescope unmodeled errors	0.025	$\mu\text{as}$	
Orbital velocity uncertainty	0.014	$\mu\text{as}$	Reference [42]
Roll-coupled zero-point errors	0.01	$\mu\text{as}$	Table F1
Readout (RO) noise error, AC and telescope	0.051	$\mu\text{as}$	
Readout noise plus scale factors	0.076	$\mu\text{as}$	
Two inst sets and two axes	0.038	$\mu\text{as}$	
RO+Orb VEI Unc+roll errors	0.041	$\mu\text{as}$	
Measure at begin and end of experiment	0.059	$\mu\text{as}$	
Subtraction error with 2 sats	0.083	$\mu\text{as}$	Total readout error
Experiment error, 1 yr	0.15	$\mu\text{as}$	RSS $2^{1/2} \times$ drift and total RO
Experiment error, 10 yr	0.048	$\mu\text{as}$	10 measurements
Geodetic relative error, 1 yr	$1.5 \times 10^{-8}$		Base is $2 \times$ geodetic drift
Geodetic relative error, 10 yr	$4.8 \times 10^{-9}$		$\approx 10$ arcsec
Error in $ 1-\gamma $ , 1 yr	$2.3 \times 10^{-8}$		Five orders of magnitude
Error in $ 1-\gamma $ , 10 yr	$7.1 \times 10^{-9}$		below current limit
$\omega_{\text{JBD}}$ , 1 yr	$4.4 \times 10^7$		Lower bound
$\omega_{\text{JBD}}$ , 10 yr	$1.4 \times 10^8$		

racy and can typically determine satellite velocity to about  $2 \times 10^{-5}$  m/sec [42]. This makes orbital aberration the precision angle standard of the experiment, which in turn depends on precision satellite, lunar, and planetary ephemerides. This technique is also part of the GP-B base line, and the approach of calibrating the large-angle instrument [the telescope here and the superconducting quantum interference device (SQUID) for GP-B] was taken from GP-B.

The actual calibration consists of modeling the errors with a calibration polynomial or some other set of functions which describes them as a function of the  $x$  and  $y$ -input angles. Since the two instrument axes could possibly be cross coupled, it is necessary to have both  $x$ - and  $y$  terms in the calibration of a given axis. If  $x$  and  $y$  are the inputs and  $m_x$  is the output of the  $x$  axis of an instrument, then a typical third-order calibration polynomial would have the form  $m_x = a_1 + (1 + a_2)x + a_3y + a_4x^2 + a_5xy + a_6y^2 + a_7x^3 + a_8x^2y + a_9xy^2 + a_{10}y^3$ , where the  $a_i$  are of the order of  $10^{-4}$ . For the relativity-gyroscope experiment, the questions become, how much calibration time is available, how many calibration points can be taken in this time, what accuracy is possible with this number of points, at what order should the

calibration polynomial be cut off, and what are the errors introduced by the unmodeled terms beyond the cutoff order? It is shown in Appendix G that it is sufficient to perform the calibration through third order. The reason is that all even-order terms ( $a_1$ ,  $a_4$ ,  $a_5$ ,  $a_6$ , etc.), not just the zero-point error  $a_1$ , are separated from the data by the satellite spin, and with a third-order calibration polynomial, the unmodeled terms are fifth order and higher. The conclusion of Appendix G is that a third-order model achieves an accuracy of  $0.03 \mu\text{as}$  after  $4 \times 10^6$  data points (i.e., six months of calibration) and that the additional error caused by the unmodeled higher-order odd terms is about  $0.05 \mu\text{as}$  at full scale.

## VII. OVERALL EXPERIMENT ACCURACY

Table IV shows the experiment errors and the calculation of the final overall errors for the measurement of  $1-\gamma$  or equivalently of  $\omega_{\text{JBD}}$ . The drift and readout errors are first listed separately and then later combined. The readout noise averaging time comes from the fact that passes in null last a minimum of 180 sec at the beginning of the experiment and 900 sec at the end, but only about one-half of this time is

### Experiment Errors

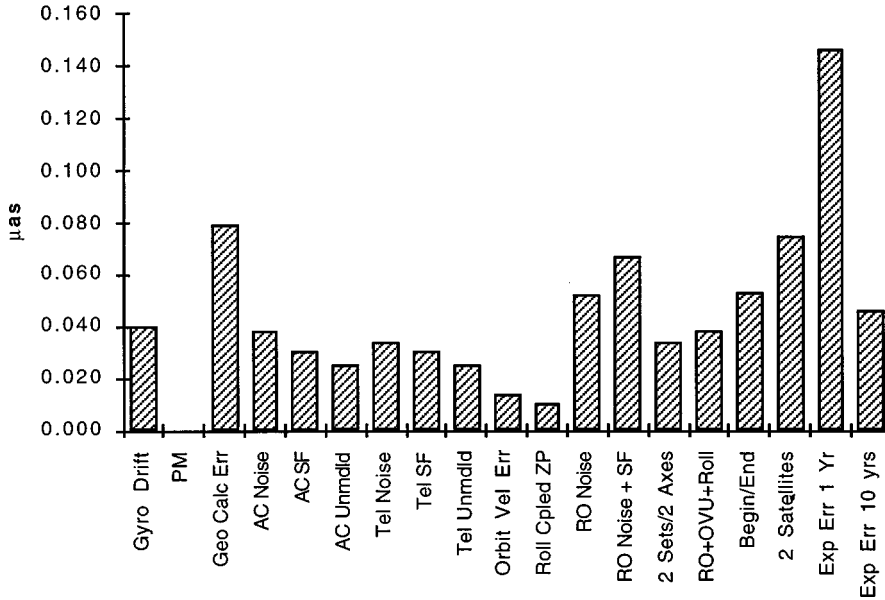


FIG. 4. Summary of experimental errors.

accessible for averaging since the peak null of  $\pm 0.2$  arcsec is not available the whole time. The effective telescope noise averaging time is the reciprocal of the average of the reciprocals of one-half of the start and end times in null. For the scale-factor errors, the weighted third-order curve of Fig. G1 and about one-half of the unmodeled errors are used because the readout does not spend all of its time at full scale. The averaged errors are then reduced 2 times by a factor of  $2^{1/2}$  since there are two independent sets of instruments and each instrument has two axes which essentially measure the same quantity because of the roll. The aberration error due to the uncertainty in the orbital velocity and the zero-point errors at roll, however, are not considered to be uncorrelated and are therefore combined with the previous result without reducing them by 2. The readout errors are then increased 2 times by  $2^{1/2}$  because there are two measurements at the beginning and the end of an experiment and because the final signal is generated by subtracting the results of the two satellites to eliminate proper motion. The gyroscope drift and geodetic calculation errors ( $\times 2^{1/2}$  for two satellites) are then included to give the final error in a single 1-yr experiment. The gyroscope alignment error is covered by the initial readout error.

The relative error is calculated by dividing by 10 arcsec, 5 arcsec for each satellite, which is consistent with increasing the overall error by  $2^{1/2}$  because of the subtraction of the two measurements. The 10-yr errors assume that the experiment is repeated 10 times in altitude increments of 100 km and that no variation from the  $r_s^{-5/2}$  altitude dependence is detected. In this case the 10-yr average is the 1-yr average divided by  $10^{1/2}$ . The final result is that  $1-\gamma$  can be measured to less than one part in  $10^8$ . Figure 4 shows a summary of the errors as a bar graph.

### VIII. RESOLVING THE DISCREPANCY WITH GP-B

It is claimed that the AC-USG is  $10^3$ – $10^4$  times more accurate than a helium-temperature design based on electri-

cally supported gyroscopes read out by a SQUID magnetometer (SQUID-ESG). How can this much improvement be possible? A much more direct form of this question can be posed: How is it possible to improve on the GP-B experiment by 3 or 4 orders of magnitude when so many people have looked at it, when it has been discussed at many conferences, and when more than 30 Ph.D theses have been written on various problems associated with the project? This is a question which it seems that almost anyone would ask, and it deserves a careful response. The short answer is that early in the GP-B program the constraint that the experiment be performed at low temperatures was imposed on the project, and when this constraint is removed, the possibilities of high accuracy open up naturally. To really resolve the discrepancy, however, it is necessary to compare the two designs point by point. There are still the same four basic items to investigate: gyroscope drift, gyroscope readout error, telescope error, and zero-point errors at roll frequency. In addition, two other points—taking data in null and multiple measurements versus altitude—are examined.

#### A. Gyroscope drift

The biggest improvement in drift comes about through better roll averaging caused by controlling the satellite spin to be parallel to the gyroscope instead of pointing to the star. GP-B does not use the gyroscope as an attitude reference because it is difficult to employ mechanisms in the cryogenic telescope with the result that the telescope cannot tolerate the large deviations from null which would be caused by the annual aberration. On the other hand, GP-B must take data at large aberration angles since averaging over the entire year is necessary to achieve the desired accuracy.

In addition to improved roll averaging, the use of an unsupported gyroscope results in only about 24 sources of spurious drift torques compared to over 70 for the ESG, and the gap is about 300 times larger. In addition, the cavity of the

AC-USG is smoothly spherical, whereas the GP-B cavity contains the gas spin-up channel. The results is that the calculated gyroscope drift for GB-B is about 4000 times worse than the AC-USG drift for the ESGs and 400 times worse for the GP-B USG,<sup>9</sup> and in addition the results of the 1972 drag-free flight have little relevance for the GP-B cavity design.

### B. Gyroscope readout errors

One of the most important reasons for the greatly increased accuracy of the AC-USG is that an autocollimator is a much more sensitive angle measuring device than a SQUID magnetometer. The noise-equivalent angle of the SQUID is about 0.19 arcsec/Hz<sup>1/2</sup> [44,45,46]. This is about 20 000 times larger than the autocollimator. The reason for this is that the London moment is very tiny, corresponding to a uniform field in the rotor of  $10^{-4}$  G at a spin speed of 130–150 Hz. An accuracy of  $10^{-9}$  rad (0.2 mas) demands that the SQUID be able to detect  $10^{-13}$  G and that there be no disturbing magnetic fields at roll frequency any larger than  $10^{-13}$  G.

One important disturbing signal for the SQUID readout is magnetic flux trapped in the rotor. The GP-B rotors have about  $10^{-5}$  G cm<sup>2</sup> of trapped flux, which corresponds to a magnetic field of  $10^{-6}$  G for a diameter of 3.8 cm [44,45,46].  $10^{-6}$  G is equivalent to 1800 arcsec or  $0.5^\circ$  for a London moment of  $10^{-4}$  G. Although this is separated from the data signal by the rotor frequency, it is still about  $10^7$  times larger than the desired accuracy of the system. In spite of this very large disturbance, a recent analysis has shown that the accuracy goal of 0.2 mas can still be met with 1 yr of continuous averaging [46]. Furthermore, a continuing effort is being made to reduce the trapped flux (cf. the GP-B papers from the Eighth Marcel Grossmann meeting). It is very unlikely, however, that this readout method could ever reach microarcsecond levels.

### C. Telescope readout errors

Since the AC-USG telescope is not placed in a cryostat, it can be about 3 times larger, and this reduces the noise-equivalent angle of the instrument by about a factor of 10. An additional factor of 2 is gained by the less stringent IR-window attenuation requirements, and a further factor of 10 can be achieved by using the brightest stars. GP-B does not use the bright stars because of the large uncertainties in their proper motions, and without the counterrotating orbits, it must rely on stars whose proper motion has been determined to be at least 200  $\mu$ as/yr. In practice, this means the fifth-magnitude VLBI radio stars whose proper motion will prob-

ably soon be known to about 100  $\mu$ as/yr [37,43], but still about a factor of 1000 bigger than the requirement for the AC-USG.

### D. Roll-frequency zero-point errors

Since the AC-USG satellite spin rate is about 30 times faster than the GP-B spin rate, there is a considerable reduction in the amplitude of roll-frequency temperature variations from this source. This can be seen from Fig. F1, which shows that although this problem can be solved with sufficient insulation, there can be many orders of magnitude difference in attenuation over a frequency range of 30. This is due to the fact that the frequency dependence occurs in the argument of an exponential. GP-B does not spin very much faster because the centrifugal force from the spin induces additional drift in the ESGs which rises as the square of the spin speed. In addition to the spin rate difference, the sensitivity of well-designed optics to temperature is about 0.1 arcsec/K/m compared to 10 arcsec/K for the SQUID magnetometer [44]. *Since the size of the autocollimator is about 0.1 m, the autocollimator is about 100–1000 times less sensitive to temperature variations at roll than the SQUID.*

### E. Taking data in null

GP-B would have difficulty taking data in null because the gas-spin-up system for the gyroscope is a one-time device without provision for applying the precision alignment torques necessary for a good null. Fine alignment from the electric suspension torques is tentatively planned, but the final alignment error is still expected to be about 10 arcsec [45,46]. In addition, the trapped flux makes it difficult to achieve a good null since its  $0.5^\circ$  signal is far outside of the useful null range of 1.5 arcsec at 650 km.

### F. Multiple measurements versus altitude

The GP-B design is excluded from making multiple measurements versus altitude because the liquid helium only lasts for about 16 months and because the very large mass of the Dewar and liquid helium precludes adding a propulsion system to change altitude. In addition, the “one-shot” nature of the gas spin-up makes it impossible to stop the gyroscopes, change the altitude, and then respin them.

### G. Overview

The common thread which runs through this comparison is that the use of liquid helium temperatures places constraints on the design which block the use of most of the techniques which can lead to high accuracy. In addition, the difficulties of working at helium temperatures is the reason that 40 yr will have passed by the time the project comes to fruition in 2000. The arguments for low temperatures have varied over the years, but the four which are now given are that it allows the use of a SQUID magnetometer, which is an ultralow-noise device, it prevents zero-point drifts because materials are much more stable, it allows a high vacuum of  $10^{-14}$  Torr, and it allows a superconducting magnetic shield with an AC attenuation of  $10^{-12}$ . It is interesting to note that

<sup>9</sup>At the author’s insistence, it is now planned to operate one of the ESGs in GP-B as a USG by making it the drag-free proof mass. The result is that the theoretical drift for that gyroscope dropped from the calculated value of 150  $\mu$ as/yr for the other three ESGs to 15  $\mu$ as/yr. Because of this, the fifth sphere in the quartz block, which served only as the drag-free proof mass, has been removed from the latest version of the system.

TABLE V. Summary of techniques for achieving high accuracy.

Technique	Advantage
Drag-free satellite (DFS)	Accurate orbit
Unsupported gyroscope (USG)	Simple torque model and 1972-DFS drift bounds
Wide gap	Surface fields and large particles suppressed
Spinning satellite	Roll average drifts and eliminate zero-point errors
All measurements in null	Reduce scale factor errors
Spin attitude reference to gyroscope not star	Improve roll averaging by $10^3-10^4$
Autocollimator (AC) gyroscope readout	High accuracy, small, light weight, and standard
Continuous AC calibration from flats	Highly stable calibration signal
Active damper	Fast spin-up and alignment
Eddy-current induction spin-up motor	Standard motor, fast spin, reusable, good alignment
Active mass/inertia trim	All zero points coincide
Transcollimator translation readout	Very low noise and wide gap with AC technology
Tipping plate, encoder, analog divider	High accuracy with standard techniques
Rotor charge control	Reduced to practice by GP-B [40]
Cancellation by orbital aberration	Take data in null
Calibration by orbital aberration	Highly accurate angle standard, taken from GP-B
Counterrotating experiments	Eliminate star proper-motion error
Fine-tuned orbits for gravity-gradient cancellation	Easily manufactured, high-optimum-speed rotor
Long-life mission	Repeat the experiment many times

in all of these points it is possible to find a design which improves on the advantages listed above by a factor of 100–1000. For example, the autocollimator has a noise-equivalent angle about  $10^4$  times smaller than the SQUID, the material-stability requirement is orders of magnitude less severe with a high spin rate, a vacuum of  $10^{-14}$  Torr is not needed because improved roll averaging and a more careful estimate of  $\varepsilon_{ml}$  reduce the drift from gas drag by about  $10^7$ , the SQUID sensitivity to roll temperature variations is about 100–1000 times greater than the autocollimator, without a SQUID magnetometer a magnetic shield with an AC attenuation of  $10^{-12}$  is not needed, etc.

## IX. SUMMARY

The achievements of sufficient accuracy in the gyroscope experiment to have a chance of seeing a massless scalar field or string dilaton depends on a number of techniques which are listed in Table V.

The drag-free satellite keeps the gyroscope rotor centered in the cavity without support and makes precision prediction and fine-tuning of the orbit possible without disturbances from solar radiation pressure or air drag. The unsupported gyroscope removes the need for electric support fields in the cavity and makes a wide gap possible. The wide gap eliminates the danger from surface electric fields such as the patch effect and the remote danger of a large impurity jamming into the gap. Spinning the satellite separates the instrument zero-point errors from the gyroscope-star angle and roll averages satellite-fixed gyroscope drift sources. Taking measurements in null avoids the need of precision calibration over extreme ranges. Controlling the satellite spin to the gyroscope instead of the star improves roll averaging by at least  $10^3$  and gives an attitude reference during an entire orbit.

The autocollimator provides a very-low-noise gyroscope readout with existing technology and can be continuously calibrated from the flat error. The active damper makes it possible to rapidly align the gyroscope spin axis with the normal to the optical flats on the rotor. The eddy-current induction motor works with the wide gap, can reach any gyroscope spin speed, and is crucial to precision alignment of the gyroscope, which in turn is crucial to operating the telescope within the 0.2 arcsec null. It can be used multiple times and thus allows the rotor to be spun down, the satellite altitude changed, and the rotor respun, damped, and aligned for a new run. The active mass trim makes it possible to align the satellite maximum axis of inertia with the autocollimator zero point and to align the center of mass of the satellite to the center of the cavity. The transcollimator allows precision measurement of the rotor position in the cavity with a wide gap and no electric fields using existing autocollimator technology. The tipping plate, angle encoder, and analog divider allow the star error angle to be read to high precision using standard AD converters. Rotor charge control, if needed, would prevent an important source of drift. Cancellation and calibration using the orbital aberration makes satellite tracking the precision angle standard of the experiment and allows a small linear range for the telescope. Two experiments in counter rotating orbits are necessary to eliminate proper motion of the reference star and many other errors in the quality of the incoming light (Appendix E 2). Fine-tuning the orbit suppresses gravity-gradient drift while allowing a rotor which can be easily manufactured and which reduces other sources of gyroscope drift by having a high optimal spin speed for minimum gravity-gradient drift (cf. Appendix A 1). Finally, the long-life mission allows the experiment to be repeated versus altitude giving the altitude

signature of the relativity drift, which is necessary for a unique interpretation of the results, decreases the experiment error, and allows the gyroscope drift and overall system errors to be independently cross-checked from the scatter in the data.

Using the above techniques, the error calculations in Sec. VII predict that the relativity drift can be measured to an accuracy of  $0.05 \mu\text{s}/\text{yr}$  with a series of ten 1-yr experiments. This would place an upper limit on  $|1 - \gamma|$  of  $7 \times 10^{-9}$ , which is  $3 \times 10^5$  times smaller than the present bound. Accuracies of this level are sufficient to possibly detect a massless scalar field or string dilaton. The limiting error is the inability to calculate the expected geodetic drift due to orbit tracking errors.

#### ACKNOWLEDGMENTS

I wish to thank the U.S. Air Force for its support of the early phase of this work via Contract No. AF 33 (615-1411) and my many colleagues at Stanford University for stimulating discussions during the recent development of the experiment. People who directly contributed to the Autocollimator-Unsupported Gyroscope design are William N. Blanchard, Andrew Buffington, Robert H. Cannon, Jr., Robert Clappier, Daniel B. DeBra, Richard F. Deimel, C. W. Francis Everitt, Marin Falieri, Alan Fleming, F. E. Futtere, Gaylord Green, Kenneth Lorell, Howard L. McKinley, Jr., Reinhold Meisinger, Bradford Parkinson, Robert Victor Plank, J. David Powell, Leonard I. Schiff, Richard A. VanPatten, and Frankie Wong. I also wish to acknowledge extensive conversations with Professor Thibault Damour of the Institut des Hautes Etudes Scientifiques concerning the significance of the experiment.

#### APPENDICES

The following Appendices for this paper had been archived in the Electronic Physics Auxiliary Publication Service (E-PAPS) [47].

##### APPENDIX A

Calculation of the Major Gyro Drifts

##### APPENDIX B

Zero-Gravity-Gradient Orbits

##### APPENDIX C

Autocollimator Performance

##### APPENDIX D

Summary of the Technique for Placing the Optical Flats on the Rotor

##### APPENDIX E

Telescope Performance

##### APPENDIX F

Roll-Coupled Zero-Point Errors and Drifts

##### APPENDIX G

Instrument Scale-Factor Calibration Accuracy

##### APPENDIX H

Operational and Miscellaneous Considerations

- 
- [1] B. Lange, *Phys. Rev. Lett.* **74**, 1904 (1995).
- [2] B. Lange, "The Unsupported Gyroscope With Autocollimator Readout, a High-Accuracy Design for the Relativity Gyro Experiment," (report unpublished).
- [3] J. A. Schouten, Koninklijke Akademie van Wetenschappen te Amsterdam, *Proc.* **21:1**, 533 (1918).
- [4] A. D. Fokker, Koninklijke Akademie van Wetenschappen te Amsterdam, *Proc.* **23:1**, 729 (1920).
- [5] W. de Sitter, *Mon. Not. R. Astron. Soc.* **77**, 155 (1916), Eq. (97), p. 172.
- [6] Kip S. Thorne, in *Near Zero*, edited by J. D. Fairbank *et al.* (Freeman, New York, 1988), pp. 573–586.
- [7] G. E. Pugh, WSEG Research Memo No. 11, Weapons Systems Evaluation Group, The Pentagon, Washington, DC, 1959.
- [8] L. I. Schiff, *Phys. Rev. Lett.* **4**, 215 (1960); *Proc. Natl. Acad. Sci. USA* **46**, 871 (1960).
- [9] J. Lense and Hans Thirring, *Phys. Z.* **19**, 156 (1918); Hans Thirring, *ibid.* **19**, 33 (1918).
- [10] C. M. Will, *Theory and Experiment in Gravitational Physics*, revised ed. (Cambridge University Press, Cambridge, England, 1993).
- [11] Pascual Jordan, *Schwerkraft und Weltall*, 2nd ed., Die Wissenschaft, Band 107 (F. Vieweg, Braunschweig, 1955).
- [12] C. Brans and R. H. Dicke, *Phys. Rev.* **124**, 925 (1961).
- [13] Peter G. Bergmann, *Int. J. Theor. Phys.* **1**, 25 (1968); Robert V. Wagoner, *Phys. Rev. D* **1**, 3209 (1970); K. Nordvedt, *Astrophys. J.* **161**, 1059 (1970).
- [14] R. D. Reasenberg *et al.*, *Astrophys. J. Lett. Ed.* **234**, L219 (1979).
- [15] D. S. Robertson *et al.*, *Nature (London)* **349**, 768 (1991).
- [16] G. Chapline and N. Manton, *Phys. Lett.* **120B**, 105 (1983).
- [17] E. W. Kolb, *Phys. Scr.* **T36**, 199 (1991).
- [18] T. Damour and K. Nordvedt, *Phys. Rev. Lett.* **70**, 2217 (1993).
- [19] T. Damour and K. Nordvedt, *Phys. Rev. D* **48**, 3436 (1993).
- [20] T. Damour and A. M. Polyakov, *Nucl. Phys.* **B423**, 532 (1994); *Gen. Relativ. Gravit.* **26**, 1171 (1994).
- [21] Daile La and Paul J. Steinhardt, *Phys. Rev. Lett.* **62**, 376 (1989); *Phys. Lett. B* **220**, 375 (1989); **231**, 231 (1989); Alan Guth and Erick Weinberg, *Nucl. Phys.* **B212**, 321 (1983); E. J. Weinberg, *Phys. Rev. D* **40**, 3950 (1989); Paul J. Steinhardt and Frank S. Accetta, *Phys. Rev. Lett.* **64**, 2740 (1990); J.

- Garcia-Bellido and M. Quiros, *Phys. Lett. B* **243**, 45 (1990); John D. Barrow and Keiichi Maeda, *Nucl. Phys.* **B341**, 294 (1990).
- [22] T. Damour (personal communication).
- [23] T. Damour and A. Vilenkin, *Phys. Rev. D* **53**, 2981 (1996).
- [24] B. Lange, in *Seventh Marcel Grossmann Meeting*, Proceedings, edited by Robert T. Jantzen, G. MacKeiser, and Remo Rufini (World Scientific, Singapore, 1994), pp. 1538–1541.
- [25] T. Damour and B. Pichon, *Phys. Rev. D* (to be published), astro-ph/9807176.
- [26] T. Damour and D. Vokrouhlicky, *Phys. Rev. D* **53**, 4177 (1996).
- [27] B. Lange, presented at the 8th Marcel Grossmann Meeting, Jerusalem, 1997.
- [28] Gravity Probe B: I, II, and III, in *Proceedings of the 6th M. Grossmann Meeting* (World Scientific, Singapore, 1991), pp. 1632, 382, 394; J. Turneure, *Stanford Phys. Colloquium*, 1994; Saps Buchman *et al.*, in *Seventh Marcel Grossmann Meeting* [24], pp. 1533–1535. See also the plenary talk by C. W. F. Everitt and the papers by S. Buchman, M. Meifetz *et al.*, D. Bardas, and B. Muhlfelder *et al.*, presented at the 8th Marcel Grossmann Meeting, Jerusalem, Israel, 1997.
- [29] “MiniSTEP, A Minimal-Cost Version of a Satellite Test of the Equivalence Principle,” Joint ESA-NASA Study Proposal, report, Second Issue, 1996; STEP Symposium, Pisa, Italy, 1993, ESA WPP-115, edited by R. Reinhard.
- [30] B. Lange, presented at the 8th Marcel Grossmann Meeting [28].
- [31] B. Lange, “DC Cancellation as a Method of Generating a  $t^2$  Response and of Solving the Radial Nonobservability Problem in a Concentric Free-Falling Two-Sphere Equivalence-Principle Experiment in a Drag-Free Satellite,” report (unpublished).
- [32] B. Lange, Ph.D. thesis, Stanford University, Report No. 194, 1964; *AIAA J.* **2**(9), 1950 (1964); in *Unconventional Inertial Sensors Symposium Proceedings*, Baltimore, Maryland, 1964, Third Interim Report: Advanced Research in Guidance, Control, and Instrumentation, 1996; Stanford Engineering Library (SUAA-6604) or AFAL Wright-Patterson AFB (TECE-39860).
- [33] B. Parkinson and B. Lange, *J. Spacecr. Rockets* **7**, 667 (1970); **7**, 675 (1970); B. Lange, *ibid.* **9**, 96 (1972).
- [34] R. D. Reasenberg *et al.*, *Astron. J.* **96**, 1731 (1988).
- [35] Shao, Michael (personal communication).
- [36] R. V. Jones and J. C. Richards, *J. Sci. Instrum.* **36**, 90 (1959); R. V. Jones, *ibid.* **38**, 37 (1961).
- [37] J.-F. Lestrade (private communication).
- [38] W. M. Fairbank, C. W. F. Everitt, D. B. DeBra, and J. A. Lipa, “A Report on a Program to Develop a Gyro Test of General Relativity in a Satellite and Associated Control Technology,” “The Green Book,” Hansen Laboratories of Physics report, Stanford University, 1980.
- [39] APL Technical Digest **12**, 2 (1973); *J. Spacecr. Rockets* **11**, 637 (1974).
- [40] S. Buchman, T. Quinn, M. Keiser, and Dale Gill, *J. Vac. Sci. Technol. B* **11**, 407 (1993); S. Buchman *et al.*, *Rev. Sci. Instrum.* **66**, 120 (1995).
- [41] E. Myles Standish, NASA Jet Propulsion Laboratories (personal communication).
- [42] George W. Davis, Center for Space Research (CfSR), University of Texas at Austin (personal communication).
- [43] B. Lange, “The GP-B Reference Star,” GP-B Technical Report No. S0194, 1993; “Noise Equivalent Angles and Detector Current Levels for the VLBI Radio Stars and Rigel by the Method of Spectral Integration,” GP-B Technical Report No. S0225, 1994.
- [44] Presentation hard copy for the National Research Council of the National Academy of Sciences 1994 Review of GP-B (unpublished).
- [45] B. Muhlfelder, J. M. Lockhart, and G. M. Gutt, presented at the Cospar Symposium, 1996.
- [46] G.T. Haupt, Ph.D. thesis, Institution, SUDAAR Report No. 676, 1996.
- [47] See AIP Document No. E-PAPS E-PRVDAQ-59-053908 for appendices listed at the end of this paper. E-PAPS document files may be retrieved free of charge from our FTP server (<http://www.aip.org/epaps/epaps.html>) or from <ftp.aip.org> in the directory/epaps/. For further information: e-mail: PAPS@aip.org or fax: 516-576-2223.